ChemPubSoc Europe

DOI: 10.1002/chem.201403985

CHEMISTRY A European Journal Full Paper

Asymmetric Catalysis |*Hot Paper*|

Palladium–N-Heterocyclic Carbene (NHC)-Catalyzed Asymmetric Synthesis of Indolines through Regiodivergent C(sp^3)–H Activation: Scope and DFT Study

Dmitry Katayev,[a] Evgeny Larionov,[a] Masafumi Nakanishi,[a] Céline Besnard,[b] and E. Peter Kündig*[a]

Abstract: Two bulky, chiral, monodentate N-heterocyclic carbene ligands were applied to palladium-catalyzed asymmetric C–H arylation to incorporate C(sp^3)–H bond activation. Racemic mixtures of the carbamate starting materials underwent regiodivergent reactions to afford different *trans*-2,3-substituted indolines. Although this C_{Ar}–C_{alkyl} coupling requires high temperatures (140–160 °C), chiral induction is high. This regiodivergent reaction, when carried out with enantiopure starting materials, can lead to single structurally different enantiopure products, depending on the catalyst chirality. The C–H activation at a tertiary center was realized only in the case of a cyclopropyl group. No C–H activation takes place alpha to a tertiary center. A detailed DFT study is included and analyses of methyl versus methylene versus methine C–H activation is used to rationalize experimentally observed regio- and enantioselectivities.

Introduction

Transition-metal-catalyzed C–H functionalization has emerged as a powerful tool in organic chemistry. Its primary impact is that it enables heretofore inert C–H groups to become functional entities, and thereby, rendering prefunctionalization of starting materials redundant. This reduces the number of steps and opens the way to new strategies in synthesis. A number of approaches have strongly contributed to the success. The C–H bond functionalization can take place through an outer- or inner-sphere mechanisms. The former includes C–H insertions of metal–carbene species[1] and oxidations by metal–oxo complexes.[2] The latter involves the direct insertion of a transition metal into a C–H bond, leading to the formation of an organometallic intermediate (M–C bond). Long limited to C_{Ar}–H bonds and with the majority of examples being heteroatom-directed coordination/activation processes,[3] recent results have demonstrated that inner-sphere processes are also suitable for the functionalization of C(sp^3)–H bonds. Given the large number of C–H bonds in organic molecules and their high bond energies, the biggest challenge in all direct C–H functionalization approaches is selectivity. The *ortho*-directing groups have been widely used in C_{Ar}–H functionalization and the avoidance of steric congestion is a dominant factor in other reactions. The catalytic step for the formation of a carbon–metal bond from a carbon–hydrogen bond generally requires the assistance of an internal base; carboxylate ligands are used frequently. The process is described as a carboxylate-mediated concerted metalation–deprotonation (CMD) pathway.[4]

Recent reviews showed that the vast majority of these inner-sphere C(sp^3)–H activation reactions involved allylic- or benzylic C–H bonds; those alpha to a heteroatom or methyl C–H bonds.[4e,5,6] The functionalization of unactivated methylene C–H bonds through metal insertion is very rare. These are, however, arguably the most interesting cases because in R–CH_2–R′ systems the hydrogen atoms are enantiotopic. Asymmetric catalytic C–H functionalization in such systems is a very ambitious project and a worthwhile challenge. A literature precedent for a Pd–PCy_3/pivalate-catalyzed (Cy = cyclohexyl) intramolecular methylene C–H/aryl coupling to afford 2-substituted and 2,3-*trans*-fused indolines attracted our attention.[7] Subsequently, we and others demonstrated that this reaction could be carried out to give highly enantioenriched products. The key to success in this asymmetric methylene coupling in our hands was the use of monodentate chiral N-heterocyclic carbene (NHC) ligands (Scheme 1).[8] An impressively wide array of highly enantioenriched, substituted indolines and azaindolines was made available by this route.

The groups of Kagan[9] and Cramer[10] chose the chiral phosphine ligands Duphos and Sagephos, respectively; the latter

[a] *D. Katayev,[+] Dr. E. Larionov,[+] Dr. M. Nakanishi,[+] Prof. Dr. E. P. Kündig*
Department of Organic Chemistry, University of Geneva
30 Quai Ernest Ansermet, 1211Geneva 4 (Switzerland)
Fax: (+)4122-237-3215
E-mail: peter.kundig@chiorg.unige.ch

[b] *Dr. C. Besnard*
Laboratoire de Crystallographie, University of Geneva
Quai Ernest Ansermet 24, 1211 Geneva 4 (Switzerland)

[+] *These authors contributed equally to this work.*

Supporting information for this article is available on the WWW under http://dx.doi.org/10.1002/chem.201403985. It contains experimental, spectroscopic, analytical, computational, and X-ray data.

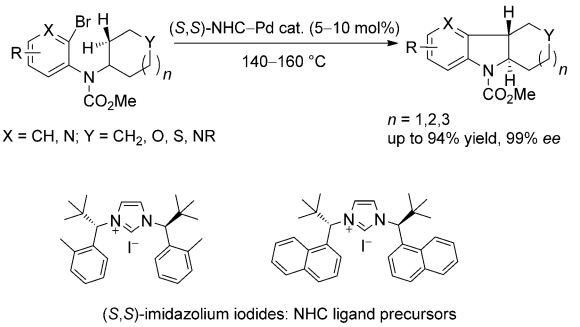

Scheme 1. Indoline synthesis through asymmetric C(sp^3)–H activation.

outperformed the former. Related research, aimed at substituted chiral indanes, was published by Baudoin et al.[11]

Experimental studies showed that a palladium-coordinated carboxylate ligand was important for the reaction and computational analysis pointed to an inner-sphere, carboxylate-assisted CMD pathway analogous to that formulated previously for C_{Ar}–H functionalization. The CMD step is rate and enantioselectivity determining in the [Pd(NHC)*]-catalyzed reaction.[12] Stoichiometric studies showed that acetate and pivalate performed best, but that even carbonate could play the role of internal base, albeit less efficiently.[12]

In probing the scope and limitations of this transformation, we found that the chiral NHC/Pd catalysts reacted with racemic starting materials by regiodivergent reaction of a racemic mixture (RRM; Scheme 2).[13,14]

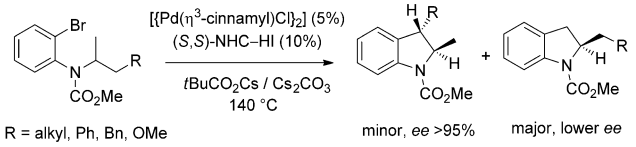

Scheme 2. The RRM through C(sp^3)–H activation.

Herein, we report on our findings on the scope and limitations in the synthesis of enantioenriched indolines through the RRM. We also demonstrate its use in synthesis with enantiopure starting materials, for which single compounds rather than mixtures can be obtained in high enantiomeric purity. In the second part of this article, we describe a DFT study to probe the CMD step of this transformation and analyze the reactivity of methyl versus methylene groups for the rationalization of the selectivity observed in regiodivergent RRM.

Results and Discussion

Starting materials **1a**–**v** were prepared by using either reductive amination of ketones with 2-bromoaniline or Buchwald–Hartwig N-arylation of primary amines with 1,2-dibromobenzene[15] followed by carbamation with methyl chloroformate. We previously found that substrate **1a** underwent an arylation reaction through C–H bond activation of both methyl and methylene units (Table 1, entry 1).[13] In this case, product (*R*)-**3a** arises from the matched case of the reaction of substrate (*S*)-**1a** and catalyst Pd–(*S*,*S*)-**4**. It is formed in higher yield, but lower enantiomeric excess (*ee*) than that of (2*R*,3*S*)-**2a** because the reaction of (*R*)-**1a** and Pd–(*S*,*S*)-**4** is the mismatched pair and gives not only (2*R*,3*S*)-**2a**, but also (*S*)-**3a**; thus lowering the *ee* value of **3a**. It is characteristic that, although the major isomer is obtained in varying enantiomeric enrichment, the minor isomer is formed uniformly in very high enantiomeric purity with only a single exception (**2g**). The difference in yield between the two indolines can be very small. The first example is the reaction of **1b**, with which C–H insertion can occur either in the methyl group (to give **3b**) or in the benzyl methylene group (to give **2b**). The enantiomer recognition by the chiral catalyst is almost perfect here. The catalyst (*S,S*)-**5** reacts with (*S*)-**1b** to give, in approximately equal proportion, two different, highly enantioenriched indolines (Table 1, entry 2).[13] It was of interest then to see the influence of a *para*-substituent on the aryl ring on the reaction outcome. These data show that 4-Me, -OMe, and -CF_3 uniformly provided excellent yields and selectivities (Table 1, entries 3–5). An erosion of yield and/or selectivity is apparent with 4-F- and 4-NO_2-substituted benzyl substrates (Table 1, entries 6 and 7). High discrimination was also observed with substrates that incorporated 2- and 3-aryl substituents, with the exception of 2-C_6H_4OMe, for which sterics may be unfavorable (Table 1, entries 8–10). Finally, in the aromatic series, we note the regiodivergent reaction also performs well with substrate **1k**, which incorporates a furyl group (Table 1, entry 11). The data in entries 12 and 13 in Table 1 show the complete absence of products **2l** and **2m**, but a high yield of **3l** and **3m,** albeit in low enantiomeric purity. Indolines **2l** and **2m** are not formed because C–H activation does not tolerate branching in the alpha position of the methylene group. In these two cases, we see that methyl activation of both enantiomers takes place. The enantiomeric enrichment of **3l** points to a degree of kinetic resolution in the transformation. Table 1, entries 14–19, list RRM results of the competition of a methyl group with chains that contain heteroatoms or an alkene functionality. We see throughout good to excellent divergent reactions for the two enantiomers in the racemic mixture, with the exception of acetyl-containing substrate **3q** (Table 1, entry 17) and the reaction of **1s** that produced **3s** with excellent enantioselectivity, but gave indene, rather than **2**, presumably because of methanethiol elimination. Entries 20 and 21 in Table 1 demonstrate that this extraordinary selectivity can also hold for reactions in which two different methylene groups are pitched against each other.

As pointed out above, the C–H activation reported herein does not tolerate branching in the alpha position of the methylene group (Table 1, entries 12 and 13), nor does it engage C–H bonds in the tertiary positions. One exception is the cyclopropyl-containing substrate **1v**, which undergoes the regiodivergent reaction with the formation of products (*R*)-**2v** and (*R*)-**3v**. Compound (*S*)-**2v** is formed through activation of the cyclopropyl methine C–H bond in (*S*)-**1v** and (*R*)-**3v** is formed through activation of the CH_3 group in (*R*)-**1v** (Scheme 3). Methine C–H activation has literature precedent.[10b,c16]

Table 1. Substrate scope for the synthesis of enantioenriched indolines through the RRM.

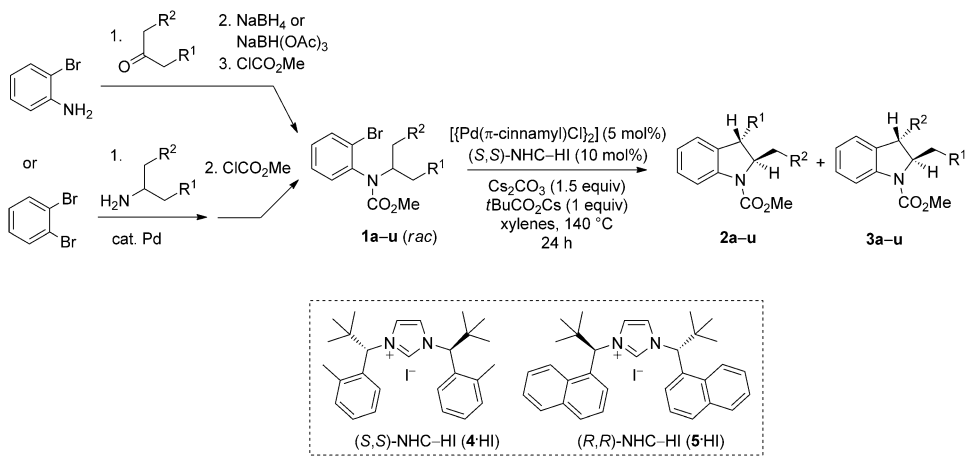

Entry[a]	Starting material	R^1	R^2	Ligand precursor NHC–HI	Product **2**[b] (yield, *ee* [%])	Product **3**[b] (yield, *ee* [%])
1[13]	**1a**	Me	H	(*S*,*S*)-**4**	(2*R*,3*S*)-**2a** (38, 99)	(2*R*)-**3a** (57, 77)
2[13]	**1b**	Ph	H	(*S*,*S*)-**5**	(2*R*,3*S*)-**2b** (44[c], 98)	(2*R*)-**3b** (49[c], 95)
3	**1c**	4-C_6H_4Me	H	(*R*,*R*)-**5**	(2*S*,3*R*)-**2c** (46, 99)	(2*S*)-**3c** (48, 94)
4	**1d**	4-C_6H_4(OMe)	H	(*R*,*R*)-**5**	(2*S*,3*R*)-**2d** (49, 99)	(2*S*)-**3d** (50, 93)
5	**1e**	4-$C_6H_4(CF_3)$	H	(*R*,*R*)-**5**	(2*S*,3*R*)-**2e** (49, 98)	(2*S*)-**3e** (49, 96)
6	**1f**	4-C_6H_4F	H	(*R*,*R*)-**5**	(2*S*,3*R*)-**2f** (32, 98)	(2*S*)-**3f** (35, 89)
7	**1g**	4-$C_6H_4(NO_2)$	H	(*R*,*R*)-**5**	(2*S*,3*R*)-**2g** (18, 68)[c]	(2*S*)-**3g** (46, 93)[c]
8	**1h**	2-C_6H_4(OMe)	H	(*R*,*R*)-**5**	(2*S*,3*R*)-**2h** (38, 99)	(2*S*)-**3h** (60, 66)
9	**1i**	2-C_6H_4F	H	(*R*,*R*)-**5**	(2*S*,3*S*)-**2i** (46, 98)	(2*R*)-**3i** (49, 93)
10	**1j**	3-C_6H_4(OMe)	H	(*R*,*R*)-**5**	(2*S*,3*R*)-**2j** (39, 99)	(2*S*)-**3j** (42, 94)
11	**1k**	2-furyl	H	(*R*,*R*)-**5**	(2*S*,3*R*)-**2k** (42, 98)	(2*S*)-**3k** (45, 97)
12	**1l**	*c*Hex	H	(*S*,*S*)-**4**	–[f]	(2*R*)-**3l** (81, 25)[c]
13	**1m**	*i*Pr	H	(*S*,*S*)-**4**	–[f]	(2*R*)-**3m** (86, 9)[c]
14	**1n**	prenyl	H	(*S*,*S*)-**4**	(2*R*,3*S*)-**2n** (29, 99)	(2*R*)-**3n** (51, 70)
15	**1o**	CH_2OMe	H	(*S*,*S*)-**4**	(2*R*,3*S*)-**2o** (35, 99)[c]	(2*S*)-**3o** (51, 85)[c]
16	**1p**	CH_2OMOM	H	(*S*,*S*)-**4**	(2*R*,3*S*)-**2p** (44, 99)[c]	(2*S*)-**3p** (45, 78)[c]
17	**1q**	CH_2OAc	H	(*S*,*S*)-**4**	(2*R*,3*S*)-**2q** (42, 96)[c]	–[f]
18	**1r**	CH_2SMe	H	(*S*,*S*)-**4**	(2*R*,3*S*)-**2r** (29, 95)[c]	(2*S*)-**3r** (56, 74)[c]
19	**1s**	SMe	H	(*S*,*S*)-**4**	–[f]	(2*S*)-**3s** (45, 97)[c,e]
20	**1t**	Me	Ph	(*S*,*S*)-**4**	(2*R*,3*S*)-**2t** (43, 99)	(2*R*,3*S*)-**3t** (47, 90)
21[d]	**1u**	OMe	Me	(*S*,*S*)-**4**	(2*R*,3*S*)-**2u** (40, 96)	(2*S*,3*S*)-**3u** (40, 88)

[a] Conditions: substrate (0.2 mmol), NHC–HI (10 mol%), [{Pd(π-cinnamyl)Cl}$_2$] (5 mol%), cesium pivalate (1 equiv), and Cs_2CO_3 (1.5 equiv) were used in dry xylenes at 140 °C for 24 h. [b] Determined by ^{1}H NMR spectroscopic analysis of an isolated mixture **2**/**3**. [c] Yield of product isolated. [d] Conditions: (*S*,*S*)-**5** (5 mol%), [{Pd(π-cinnamyl)Cl}$_2$] (2.5 mol%), cesium pivalate (1 equiv), and Cs_2CO_3 (1.5 equiv) in dry mesitylene as a solvent at 160 °C for 3 h. [e] Indole was a side product. [f] No product detected.

enantioenriched products can be obtained either by using the same catalyst on different enantiomers of the starting material or by switching the chirality of the catalyst. The former is demonstrated by the example given in Scheme 4 and the latter is shown in Table 2. The requisite enantiopure substrates **1b**, **u**, and **w**–**y** were synthesized through palladium-catalyzed Buchwald–Hartwig N-arylation of primary amines with 1,2-dibromobenzene[15] followed by carbamation with methyl chloroformate.

Entries 1–8 in Table 2 depict competitive methylene C–H coupling reactions with extraordinarily high regio- and diastereoselectivity. The products are entirely under the control of the catalyst. Reactions with the (*R*,*R*)-catalyst led to the asymmetric functionalization of a $C_{methylene}$–H bond adjacent to the OMe group to afford products **2u**, **w**, and **x**, whereas the (*S*,*S*)-catalyst engaged a $C_{methylene}$–H bond of the alkyl side chain to afford products **3u**, **w**, and **x**. Entries 7 and 8 in Table 2 lead to analogous highly selective coupling reactions that involve either a CH_3 group or the CH_2 group adjacent to

In the optimum case, the RRM reactions afford two enantiopure regioisomeric products in 50% yield each. Although fascinating, their use in synthesis is limited because of the need for product separation.

However, when starting from enantiopure precursors, this limitation disappears and in selected examples single, highly

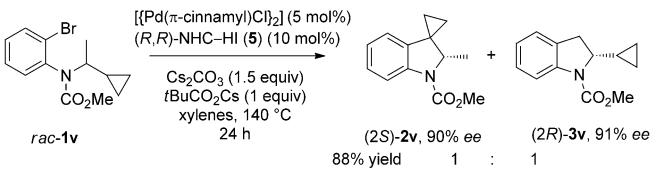

Scheme 3. Divergent C–H activation: methine versus methyl C–H bonds.

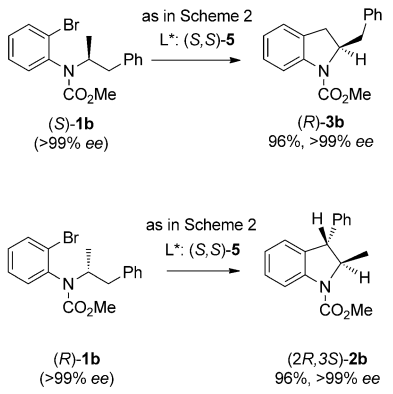

Scheme 4. Enantiomers reacting with identical catalysts to give regiodivergent single products.

Table 2. Switching the chirality of the catalyst, which leads to regioisomeric enantiomerically pure products.

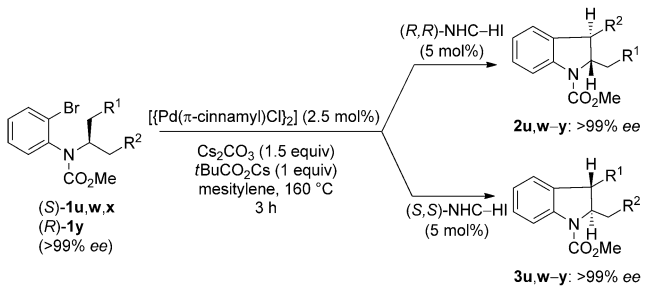

Entry	R^1/R^2	Starting material	NHC–HI	Product **2** (yield[b], *ee* [%])	Product **3** (yield[b], *ee* [%])
1[a]	Me/OMe	**1u**	(*R*,*R*)-**5**	(2*S*,3*R*)-**2u** (86, >99)	not formed
2[a]	Me/OMe	**1u**	(*S*,*S*)-**5**	not formed	(2*S*,3*S*)-**3u** (85, >99)
3[a]	Et/OMe	**1w**	(*R*,*R*)-**5**	(2*S*,3*R*)-**2w** (97, >99)	not formed
4[a]	Et/OMe	**1w**	(*S*,*S*)-**5**	not formed	(2*S*,3*S*)-**3w** (96, >99)
5[a]	Ph/OMe	**1x**	(*R*,*R*)-**5**	(2*S*,3*R*)-**2x** (98, >99)	not formed
6[a]	Ph/OMe	**1x**	(*S*,*S*)-**5**	not formed	(2*S*,3*S*)-**3x** (98, >99)
7[c]	3-*N*-Me indolyl/H	**1y**	(*R*,*R*)-**4**	(2*S*)-**2y** (88, >99)	not formed
8[c]	3-*N*-Me indolyl/H	**1y**	(*S*,*S*)-**4**	not formed	(2*R*,3*S*)-**3y** (77, >99)

[a] Conditions: substrate (0.2 mmol), NHC–HI (5 mol%), [{Pd(π-cinnamyl)Cl}$_2$] (2.5 mol%), cesium pivalate (1 equiv), and Cs_2CO_3 (1.5 equiv) were used in dry mesitylene (2 mL) at 160 °C for 3 h. [b] Yield of product isolated. [c] Conditions: (*R*)-**1y** (0.2 mmol), NHC–HI (10 mol%), [{Pd(π-cinnamyl)Cl}$_2$] (5 mol%), cesium pivalate (1 equiv), and Cs_2CO_3 (1.5 equiv) were used in dry xylenesxyleness (2 mL) at 140 °C for 24 h.

the indolyl fragment. As before, only 2,3-*trans*-disubstituted indolines were formed.

Recrystallization of enantiopure indoline (2*S*,3*S*)-**3x** from a solution in hexane and ethyl acetate afforded crystals suitable for X-ray analysis. The structure is shown in Figure 1 and clearly demonstrates that the *trans* configuration of the 2,3-disubstituted indoline is formed. This is in perfect agreement with the results previously obtained from vibrational circular dichroism (VCD) studies.[13]

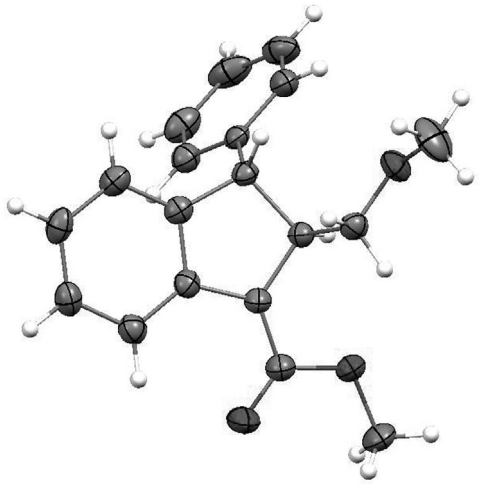

Figure 1. X-ray structure of *trans*-indoline (2*S*,3*S*)-**3x**.[17] Ellipsoids are given at the 50% probability level.

The proposed reaction mechanism is shown in Scheme 5. The Pd^0–NHC catalyst is formed by treatment of [{Pd(π-cinnamyl)Cl}$_2$] and NHC–HI with cesium pivalate as a base and nucleophile. Oxidative addition of aryl bromide to the Pd^0–carbene complex fragment produces palladacycle **A** as a key intermediate. Bromide exchange for pivalate sets the stage for the asymmetric regiodivergent step by C(sp^3)–H activation through a pivalate-assisted CMD reaction.[12,16] The two palladacycles produce the indolines by reductive elimination; thus closing the catalytic cycle. In a preliminary article, we showed that methyl C–H activation was favored over methylene C–H activation with the achiral catalysts Pd–IMes or Pd–PCy_3 (IMes = 1,3-dimesitylimidazol-2-ylidene; both give *rac*-**3a** exclusively). The energy difference of the two transition states appears to be small enough to be overcome when a suitable chiral ligand (e.g., **4** or **5**) is employed. This warranted further analysis and led to the computational study detailed below.

Computational study

Our recent combined theoretical and experimental study showed that the Pd–NHC-catalyzed C(sp^3)–H arylation proceeded through a CMD mechanism.[4,12] The CMD step for the activation of *N*-isopropyl carbamate was shown to be selectivity determining. In view of the results detailed in the first part of this article, we proceeded with a detailed DFT study of methyl versus methylene C(sp^3)–H activation to rationalize selectivities observed in the regiodivergent reaction of racemic mixtures.[4c–e,18] The computed activation barriers ($\Delta G^{\ddagger}_{413}$, gas phase) for the CMD step with a truncated achiral NHC ligand and calculated for the activation of **1a** are as follows: CH_3 (118.4 kJ mol^{-1}) < $CH_{2\,trans}$ (129.4 kJ mol^{-1}) < $CH_{2\,cis}$ (149.3 kJ mol^{-1}).[19] This is in agreement with the finding that Pd–IMes or Pd–PCy_3 exclusively give the indoline that results from CH_3/Ar coupling.[12] We note, however, that $\Delta\Delta G^{\ddagger}_{413}$ $CH_3/CH_{2\,trans}$ in **1a** computes to merely 11.0 kJ mol^{-1}. A chiral ligand may overcome this difference. For the methyl versus methine C–H activation in **1v**, the numbers are $CH_{cyclopropyl}$ (122.7 kJ mol^{-1}) < CH_3 (129.0 kJ mol^{-1}) < $CH_{2\,trans}$ (138.9 kJ mol^{-1}) < $CH_{2\,cis}$ (150.8 kJ mol^{-1}). Here, $\Delta\Delta G^{\ddagger}_{413}$ $CH_{cyclopropyl}/CH_3$ is only 6.3 kJ mol^{-1}. Again, this is a small difference and a suitable ligand may change the situation. Details of the above analyses are given in the Supporting Information. In the following section, we discuss C–H activation by the [Pd((*S*,*S*)-**4**)] catalyst.

Activation of substrate 1a

The experiments show that the coupling reaction of racemic substrate **1a** formed the two products **2a** and **3a** (Table 1, entry 1). The CH_3 activation product **3a** is present in higher yield (57%), but with lower *ee* of 77% compared with CH_2 activation product **2a**, which is formed in 38% yield with a very high *ee* of >99%. Product (*R*)-**3a** represents the matched case

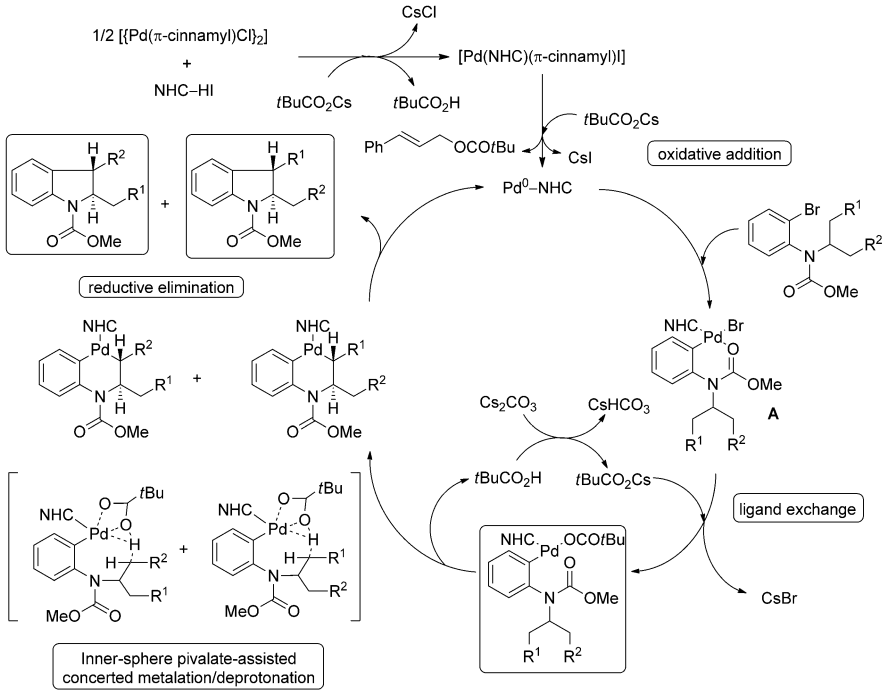

Scheme 5. Proposed catalytic cycle for the title-reaction.

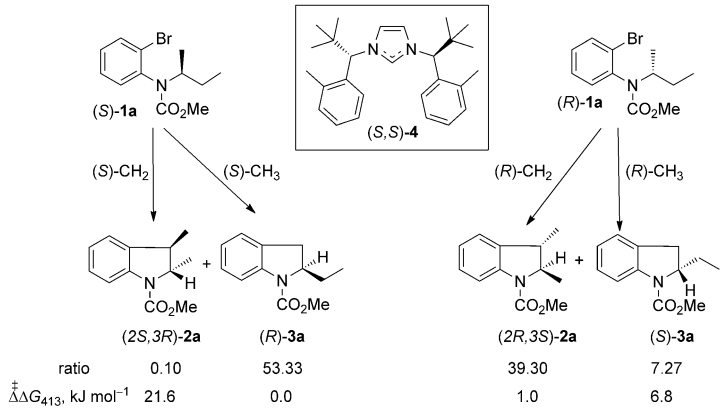

Scheme 6. Rationalization of regiodivergent RRM of substrate **1a**.

of substrate (*S*)-**1a** and catalyst Pd–(*S,S*)-**4**. It is formed in higher yield, but lower enantioselectivity because (*R*)-**1a**/Pd–(*S,S*)-**4**, which is the mismatched pair, produces not only (2*R*,3*S*)-**2a** (catalyst control, excellent enantioselectivity), but also some (*S*)-**3a** (Scheme 6). The differences in activation energies can be calculated from the relative amounts of products formed (Scheme 6).

The activation barriers of the CMD step for different pathways of C(sp^3)–H activation of carbamate **1a** were calculated (Figure 2). The results show that, with the chiral NHC, the preference for the formation of the *trans* product in CH_2 activation persists, as observed for the model achiral NHC (see the Supporting Information for details). The $\Delta\Delta G^{\ddagger}_{413}$ values for *cis*- and *trans*-CH_2 activation are 15.9 kJ mol^{-1} for (*R*)-CH_2 and 8.8 kJ mol^{-1} for (*S*)-CH_2. In agreement with experiments, CH_3 activation is preferable for (*S*)-**1a** than that for (*R*)-**1a**. The respective difference between the activation barriers for *trans*-CH_2 activation is 16.9 kJ mol^{-1} in favor of the (*R*)-CH_2 transition state (Figure 2). This is again in agreement with experimentally observed higher *ee* values of product **2a**.

The structures of the transition states *trans*-(*R*)-CH_2 and *trans*-(*S*)-CH_2 are also shown in Figure 2. As observed for C–H activation of parent *N*-isopropyl carbamate,[12] there is steric repulsion between the substrate benzene ring and an *o*-methyl group of the NHC ligand in TS *trans*-(*S*)-CH_2 (the distance between the center of the benzene ring and the *o*-methyl hydrogen is 2.321 Å), which increases the energy of the transition state. Moreover, the interaction of the second *o*-methyl group of the NHC ligand with the methyl group connected directly to the reacting carbon atom of the substrate further increases the energy of *trans*-(*S*)-CH_2; thus leading to high enantioselectivity for CH_2 activation. Interestingly, transition state *trans*-(*S*)-CH_2 is a late transition state compared with *trans*-(*R*)-CH_2. This is shown in more detail and in color in the Supporting Information, in which the graph from Figure 2 is reproduced with the inclusion of solvent effects (xylenes). Although the numbers are different, the order of calculated $\Delta G^{\ddagger}_{413}$ is the same.

Next, we attempted to correlate the activation barriers, which were calculated relative to the most stable transition state (*S*)-CH_3, with the respective experimental values. A graphical representation of this comparison is shown in Figure 3. The results show that the free energy barriers, $\Delta\Delta G^{\ddagger}_{413}$, in the gas phase correlate very well with the experimental data ($R^2 = 0.9819$, root-mean-square deviation (RMSD) = 1.8 kJ mol^{-1}). The largest deviation from experiment (3.3 kJ mol^{-1}) is observed for transition state *trans*-(*S*)-CH_2, which leads to product (2*S*,3*R*)-**2a**. Due to the very low yield of this product (detected as a minor peak in HPLC), the error in the experimental relative free energy barrier is quite large. The inclusion of solvent effects in xylenes as polarizable continuum model (PCM) single-point calculations with united-atom Hartree–Fock (UAHF) radii does not improve the correlation significantly (see the Supporting Information).

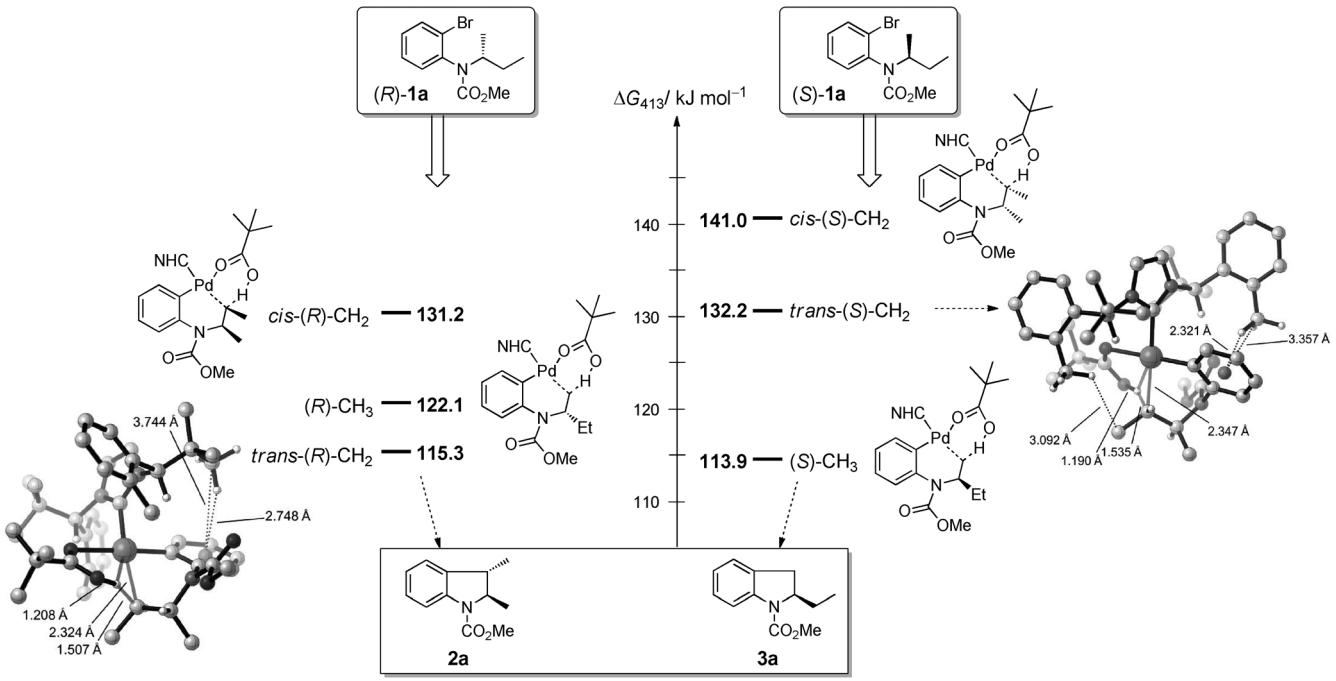

Figure 2. Activation barriers ($\Delta G^{\ddagger}_{413}$, gas phase) for the CMD step with (*S*,*S*)-NHC ligand **4** and substrate **1 a**; structures of the transition states for CH_2 activation of substrate **1 a**. Selected hydrogen atoms have been removed for clarity. The (*R*) and (*S*) descriptors refer to the configuration of substrate **1 a**. A color version of this figure is available in the Supporting Information.

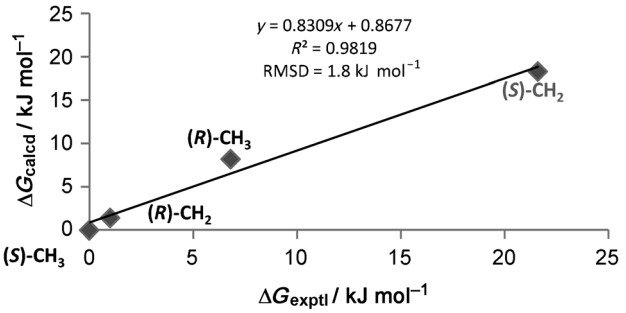

Figure 3. Correlation between experimental and calculated ($\Delta G^{\ddagger}_{413}$, gas phase) relative activation barriers for the regiodivergent RRM of substrate **1 a**.

Activation of substrate 1 b

Experimental data showed that racemic phenyl-substituted substrate **1 b** gave two products, **2 b** and **3 b**, in 1:1 ratio in intramolecular C(sp^3)–H activation (Table 1, entry 2). Both products **2 b** and **3 b** are formed in very high enantiomeric purity (98 and 95% *ee*, respectively). The activation barriers of the CMD step for the different pathways of C(sp^3)–H activation of substrate **1 b** with (*S*,*S*)-NHC ligand **4** were calculated (Figure 4). Similarly to the activation of substrate **1 a**, *trans*-product **2 b** in CH_2 activation is formed exclusively: the corresponding differences between the activation barriers for *cis*- and *trans*-CH_2 activation are 27.9 kJ mol^{-1} for (*R*)-CH_2 and 17.7 kJ mol^{-1} for (*S*)-CH_2 (see the Supporting Information).

In agreement with experimental results, compound (*S*)-**1 b** preferably undergoes CH_3 activation, whereas (*R*)-**1 b** undergoes CH_2 activation. In contrast to substrate **1 a**, transition state (*R*)-CH_3 for the activation of **1 b** is higher in energy relative to other transition states (Figure 4). Inspection of the corresponding structure shows that, in addition to steric repulsion between the substrate benzene ring and the *o*-methyl group of the NHC ligand (the distance between the center of the benzene ring and the *o*-methyl carbon is 3.313 Å), there is an unfavorable interaction between substrate phenyl and carbamate groups. This increases the energy of transition state (*R*)-CH_3; the result of which is high levels of enantioselectivity in both in CH_3 and CH_2 activation of substrate **1 b**.

The activation barriers are, in most cases, overestimated by calculations, particularly when solvent effects in xylenes are added to the gas-phase free energies (Table 3). One possible explanation for this is the systematic underestimation of dispersion interactions with the DFT functional used herein,[19] since the studied systems contain several aromatic rings. Dispersion-corrected functionals, such as B97-D, were recently shown to predict this type of interaction more accurately.[20] Therefore, we briefly studied whether using the B97-D/LANL2DZ,6-31G(d,p) level of theory for single-point calculations would improve the correlation.

Indeed, the relative activation free energies are consistently lower when calculated at the combined B97-D/M06-L level of theory, and RMSD = 4.4 kJ mol^{-1} is also lower in this case (see the Supporting Information for details). This implies that dispersion interactions play some role in the relative stability of transition states. However, the overall correlation was not better ($R^2 = 0.7707$) and full optimization at the B97-D level of theory was consequently carried out (Table 3). The obtained $\Delta\Delta G^{\ddagger}$ values at the B97-D level of theory are close to the rela-

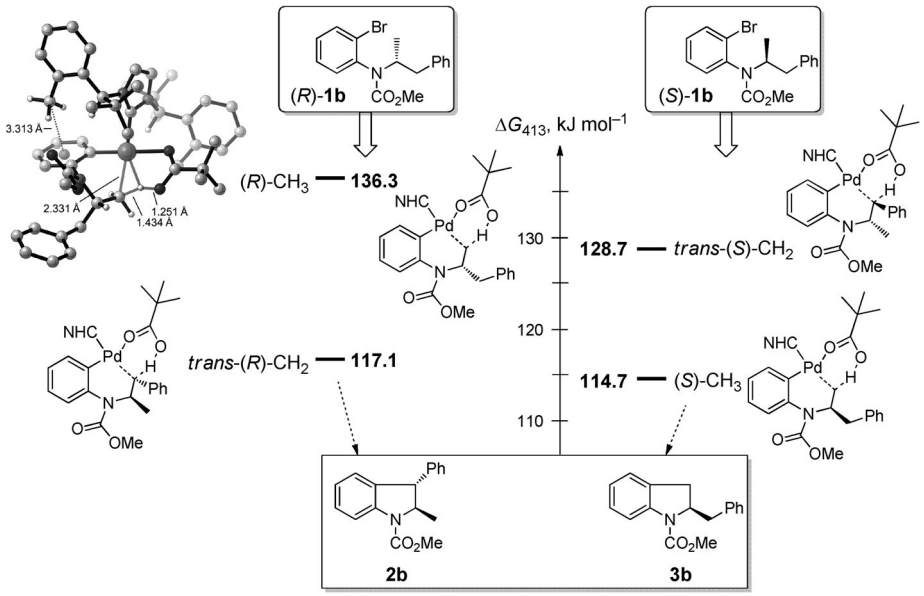

Figure 4. Activation barriers ($\Delta G^{\ddagger}_{413}$, gas phase) for the CMD step with (*S*,*S*)-NHC ligand **4** and substrate **1b**; structure of the transition state for (*R*)-CH_3 activation. Selected hydrogen atoms have been removed for clarity. The (*R*) and (*S*) descriptors refer to the configuration of substrate **1b**. A color version of this figure is available in the Supporting Information.

The results show that for *para*-methyl-substituted substrate **1c** (Ar = 4-$CH_3C_6H_4$)) the difference in $\Delta\Delta G^{\ddagger}_{413}(CH_2)$ between *trans*-(*S*)-CH_2 and *trans*-(*R*)-CH_2 activation barriers is higher and the difference in $\Delta\Delta G^{\ddagger}_{413}(CH_3)$ is lower than that for the substrate **1b** (Ar = Ph). This implies that product **2c** should be obtained in higher enantioselectivity and product **3c** should be obtained with a lower *ee* value than those of **2b** and **3b**, respectively

These predictions are in good agreement with experimental results (see Table 1, entries 2 and 3). However, the differences between the diastereomeric activation barriers are overestimated by calculations, as mentioned for substrate **1b** (see above). For

Table 3. Comparison between experimental and calculated relative activation barriers for the regiodivergent RRM of substrate **1b**.

Activation mode	Experimental $\Delta\Delta G^{\ddagger}_{413}$	Calculated $\Delta\Delta G^{\ddagger}_{413}$ [kJ mol^{-1}]		
		$\Delta\Delta G^{\ddagger}$[a] gas phase	$\Delta\Delta G^{\ddagger}$[a] xylenes	$\Delta\Delta G^{\ddagger}$[b] gas phase
(*S*)-CH_3	0.0	0	0	0
(*R*)-CH_3	9.8	21.6	19.6	20.5
trans-(*R*)-CH_2	−0.1	2.4	12.0	2.3
trans-(*S*)-CH_2	11.8	14.0	24.5	21.9
correlation coefficient R^2[c]		0.8057	0.7766	0.8874
RMSD [kJ mol^{-1}][c]		6.1	10.1	6.9

[a] Calculated at the M06-L/[LANL2DZ,6-31G(d,p)] level of theory. [b] Calculated at the B97-D/[LANL2DZ,6-31G(d,p)] level of theory. [c] Correlation coefficients, R^2, and RMSD between calculated and experimental relative activation barriers.

tive activation barriers at M06-L level, except for transition state *trans*-(*S*)-CH_2. Although the overall correlation is slightly better ($R^2 = 0.8874$), the activation barriers are, in most cases, overestimated by calculations (RMSD = 6.9 kJ mol^{-1}).

Variation of the *para* substituent in substrate 1b

To study the influence of electronic effects on enantioselectivities and product ratios in regiodivergent RRM, the activation barriers for two *para*-substituted derivatives of **1b** were calculated and compared with experimental results. The activation free energies calculated at the M06-L/[LANL2DZ,6-31G(d,p)] level in the gas phase are shown in Table 4 (for free energies in xylenes, see the Supporting Information).

Table 4. Calculated relative free energy activation barriers for the regiodivergent RRM of racemic substrates **1b**, **1c**, and **1e** with (*S*,*S*)-NHC **4**.

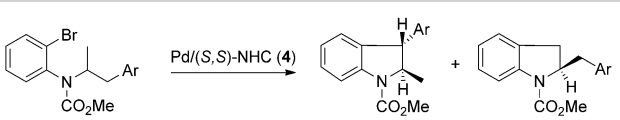

1b: Ar = Ph
1c: Ar = 4-$CH_3C_6H_4$
1e: Ar = 4-$CF_3C_6H_4$

2b, **2c**, **2e** **3b**, **3c**, **3e**

Activation mode	Calculated $\Delta\Delta G^{\ddagger}_{413}$ (gas phase)[a] [kJ mol^{-1}]		
	1b	**1c**	**1e**
(*S*)-CH_3	0.0	0.0	0.0
(*R*)-CH_3	21.6	9.6	18.1
trans-(*R*)-CH_2	2.4	−8.6	−3.8
trans-(*S*)-CH_2	14.0	17.8	9.7
$\Delta\Delta G^{\ddagger}_{413}(CH_2)$[a]	11.6	26.4	13.5
$\Delta\Delta G^{\ddagger}_{413}(CH_3)$[a]	21.6	9.6	18.1

[a] $\Delta\Delta G^{\ddagger}_{413}(CH_3) = \Delta G^{\ddagger}((R)\text{-}CH_3) - \Delta G^{\ddagger}((S)\text{-}CH_3)$; $\Delta\Delta G^{\ddagger}_{413}(CH_2) = \Delta G^{\ddagger}((R)\text{-}CH_2) - \Delta G^{\ddagger}((S)\text{-}CH_2)$.

para-trifluoromethyl-substituted substrate **1e** (Ar = 4-$CF_3C_6H_4$), the difference between *trans*-(*S*)- and *trans*-(*R*)-CH_2 activation barriers is close to the corresponding $\Delta\Delta G^{\ddagger}_{413}(CH_2)$ value for unsubstituted **1b** (Ar = Ph), so that products **3b** and **3e** are formed with the same *ee* values (Table 1, entries 2 and 5). The CH_3 activation of substrate **1e** is the only example of when computational results do not agree with those obtained experimentally: the calculated $\Delta\Delta G^{\ddagger}_{413}(CH_3)$ value is lower, but the *ee* value of **2e** is higher than that for unsubstituted product **2b**. One possible reason for this disagreement could be the different NHC ligands used in experiments (NHC **5**) and in calculations (NHC **4**).

Conclusion

We probed the scope and limitations of Pd–NHC-catalyzed asymmetric C(sp^3)–H activation that led to enantioenriched 2-substituted and *trans*-2,3-disubstituted indolines. Readily synthesized substrates that incorporated a stereogenic center were investigated and found to undergo highly regiodivergent reactions of racemic mixtures. A number of cases with enantiopure starting materials demonstrated the synthetic utility of this approach to produce single regioisomeric, enantiopure *trans*-2,3-disubstituted indolines. This is all the more remarkable because high temperatures are required to engage C(sp^3)–H bonds in coupling reactions. Limitations were that C–H bonds at, or adjacent to, tertiary centers were not touched. One exception was the methine C–H bond of a cyclopropyl moiety. A detailed DFT analysis of these reactions provided a good match to experimental data. The computational data confirmed earlier conclusions that we were in the presence of a CMD pathway and it also provided insight into the energetics of C(sp^3)–H activation of methyl–, methylene–, and methine–C–H bonds.

Experimental Section

General

Solvents were purified by filtration on drying columns by using a Solvtek system. Mesitylene was distilled over CaH_2 under nitrogen. Reactions and manipulations that involved organometallic or moisture-sensitive compounds were carried out under purified nitrogen and glassware was further dried by heating under high vacuum as necessary. Flash chromatography (FC) was performed on silica gel 60 (40 μm). Analysis with chiral HPLC was performed by using an Agilent 1100 series chromatograph with a JASCO PU-980 pump and an Agilent 1100 Series detection system.^{1}H and ^{13}C NMR spectra were recorded on a Bruker AMX-400 spectrometer; δ in ppm, pattern abbreviations: broad (b), quartet (q), quintet (quint). The Fourier transform (FT) spectrometers used an internal deuterium lock. Chemical shifts are quoted in ppm downfield of tetramethylsilane. IR spectra were recorded on a Perkin–Elmer Spectrum One spectrophotometer. Electron impact (EI) mass spectra were obtained by using Varian CH-4 or SM-1 instruments operating at 40–70 eV and electrospray ionization (ESI) HRMS analyses were measured on a VG analytical 7070E instrument. Optical rotations were measured at 20 °C on a Perkin–Elmer 241 polarimeter by using a quartz cell (l = 10 cm) with a Na high-pressure lamp (λ = 589 nm). Melting points were determined on a Büchi 510 apparatus and were uncorrected.

Dry xylenes, benzene, cesium carbonate, cesium pivalate, pivalic acid, methyl chloroformate, benzylmethylketones, and 2-bromoaniline were purchased from Sigma-Aldrich, Fluka, or Acros and used without further purification. 4-Trifluroomethylbenzylmethylketone, *N*-alkyl-2-bromoaniline derivatives,[21] and methyl *N*-alkyl-2-bromophenyl carbamates **1**[7] were prepared by following the general procedure or previously reported procedures. Carbamates **1** were obtained as mixtures of rotamers. [{Pd(π-cinnamyl)Cl}$_2$] was prepared according to a procedure reported in the literature.[22] The synthesis of the ligand precursors **4** and **5** was described previously.[23]

For full experimental data of all compounds, see the Supporting Information.

Synthesis of (*rac*)-1 v

2-Bromoaniline (3.4 g, 20 mmol, 1 equiv), 4 Å molecular sieves (6 g), and 1-cyclopropylethan-1-one (3.4 g, 40 mmol, 2 equiv) were dissolved in benzene (50 mL). The reaction mixture was heated at reflux with a Dean-Stark apparatus for 3 days and filtered through Celite. The filtrate was evaporated by rotary evaporator and dried under vacuum. The crude imine was dissolved in dry methanol (50 mL) and $NaBH_4$ (2.28 g, 60 mmol, 3 equiv) was added slowly under nitrogen. The reaction mixture was stirred for 2 h followed by addition of 1 N KOH (aq) and extraction with dichloromethane. The organic phase was dried over Na_2SO_4. After filtration and evaporation, the residue was purified by column chromatography (silica gel; diethyl ether/pentane as the eluent) to afford 2-bromo-*N*-(1-cyclopropylethyl)aniline as a yellow oil (0.72 g, 15%). ^{1}H NMR (400 MHz, $CDCl_3$): δ = 7.46 (dd, J = 7.9, 1.5 Hz, 1H), 7.19 (ddd, J = 8.2, 7.3, 1.5 Hz, 1H), 6.69–6.65 (m, 1H), 6.57 (ddd, J = 7.9, 7.3, 1.5 Hz, 1H), 4.36 (br s, 1H), 3.10 (m, 1H), 1.31 (d, J = 6.3 Hz, 3H), 1.10–0.99 (m, 1H), 0.62–0.54 (m, 2H), 0.41–0.34 (m, 1H), 0.34–0.27 ppm (m, 1H).

2-Bromo-*N*-(1-cyclopropylethyl)aniline (0.72 g, 3.0 mmol, 1 equiv) was dissolved in methyl chloroformate (3.5 mL, 45 mmol, 15 equiv). The reaction mixture was heated at reflux for 10 h before the reaction mixture was poured into ice/water and extracted with dichloromethane. The organic phase was dried over $MgSO_4$ and evaporated by means of a rotary evaporator after filtration. The crude product was purified by flash column chromatography (silica gel; ethyl acetate/pentane = 1:30 as the eluent) to afford (*rac*)-**1 v** as a colorless oil (0.54 g, 60%). ^{1}H NMR (400 MHz, $CDCl_3$): δ = 7.64 (d, J = 8.0 Hz, 1H), 7.45 (d, J = 6.9 Hz, 0.6H), 7.36–7.28 (m, 1H), 7.28–7.24 (m, 0.5H), 7.22–7.12 (m, 1H), 3.80 (m, 0.9H), 3.63 (s, 2.9H), 3.51 (d, 0.4H), 1.44 (d, J = 6.8 Hz, 1.2H), 1.17 (d, J = 6.9 Hz, 1.9H), 0.91–0.80 (m, 0.7H), 0.68–0.46 (m, 2.8H), 0.44–0.35 (m, 0.8H), 0.35–0.27 (m, 0.7H), 0.17–0.08 ppm (m, 0.4H); ^{13}C NMR (101 MHz, $CDCl_3$): δ = 156.0, 155.5, 138.3, 133.65, 133.60, 131.2, 130.6, 129.0, 128.9, 127.91, 127.87, 126.3, 126.1, 60.9, 59.7, 53.1, 53.0, 20.5, 18.0, 17.8, 15.1, 6.2, 5.6, 4.5, 4.1 ppm; IR (neat): $\tilde{\nu}$ = 2953 (w), 1704 (vs), 1585 (w), 1475 (m), 1440 (s), 1375 (m), 1315 (vs), 1262 (m), 1193 (m), 1112 (m), 1070 (m), 1044 (m), 1025 (m), 765 (s), 730 cm^{-1} (s); HRMS: *m/z* calcd for $C_{13}H_{16}BrN_1ONa$ $[M+Na]^+$: 320.0256; found: 320.0260.

Catalytic asymmetric synthesis of (2*S*)-2 v and (2*R*)-3 v

Compound (*rac*)-**1 v** (0.2 mmol, 59.4 mg), [{Pd(π-cinnamyl)Cl}$_2$] (2.6 mg, 0.005 mmol), cesium carbonate (97.5 mg, 0.3 mmol), cesium pivalate (46.8 mg, 0.2 mmol), and (*R*,*R*)-**5** (0.01 mmol, 5.88 mg) were successfully filled into a Schlenk flask. After the flask was evacuated and backfilled with nitrogen, dry xylenes (2 mL) was added and stirred at 140 °C for 24 h. The reaction mixture was cooled to room temperature and diluted with dichloromethane (2 mL) followed by filtration through Celite. The solvent was removed in vacuum and the residue was purified by flash column chromatography (silica gel; ethyl acetate/pentane system as the eluent) to afford a mixture of indolines (2*S*)-**2 v** and (2*R*)-**3 v** (38.2 mg, 88%). **2 v** + **3 v**: ^{1}H NMR (400 MHz, $CDCl_3$): δ = 8.00–7.36 (m, 1.4H), 7.24–7.13 (m, 2.3H), 7.03–6.92 (m, 1.6H), 6.66 (dd, J = 7.5, 1.3 Hz, 1H), 4.18 (br s, 1H), 4.03 (t, J = 8.6 Hz, 0.6H), 3.86 (two s, 3H + 1.8H), 3.33 (ddt, J = 15.9, 9.4, 1.2 Hz, 0.6H), 2.89–2.79 (m, 0.6H), 1.27 (d, J = 6.3 Hz, 3H), 1.20–1.06 (m, 2.6H), 1.03–0.96 (m, 1.2H), 0.88–0.80 (m, 1.2H), 0.73–0.56 (m, 0.6H), 0.58–0.40 (m,

1.2H), 0.28–0.18 ppm (m, 0.6H); **2v**+**3v**: ^{13}C NMR (101 MHz, $CDCl_3$): δ=154.4, 130.8, 127.5, 127.1, 125.01, 123.2, 123.0, 118.8, 115.8, 115.2, 77.0, 63.5, 62.2, 52.7, 52.6, 34.4, 29.9, 28.7, 20.7, 18.7, 16.6, 9.8, 4.5, 1.5, 1.3 ppm; **2v**+**3v**: IR (neat): $\tilde{\nu}$=2954 (w), 1702 (vs), 1604 (w), 1485 (m), 1440 (s), 1386 (s), 1314 (m), 1273 (m), 1192 (m), 1140 (m), 1120 (m), 1044 (m), 1055 (m), 1022 (m), 749 cm^{-1} (s); **2v**+**3v** HRMS: *m/z* calcd for $C_{13}H_{16}N_1O_2$ $[M+H]^+$: 218.1175; found: 218.1165.

Synthesis of (*S*)-1x

$[Pd_2(dba)_3]$ (2 mol%, 0.127 mmol, 116 mg; dba=dibenzylideneacetone), *rac*-2,2′-bis(diphenylphosphino)-1,1′-binaphthyl (*rac*)-BINAP; 6 mol%, 0.381 mmol, 237 mg), and *t*BuONa (0.85 g, 8.89 mmol) were successfully filled into a Schlenk flask. After the flask was evacuated and backfilled with nitrogen, dry toluene (10 mL), (*S*)-1-methoxy-3-phenylpropan-2-amine[24] (1.15 g, 6.98 mmol), and 1,2-dibromobenzene (1.5 g, 6.35 mmol) were added under nitrogen. The resulting reaction mixture was stirred at 110 °C in the Schlenk tube for 24 h. The reaction mixture was cooled to RT and diluted with ethyl acetate (20 mL) followed by filtration through a pad of Celite. The solvent was removed in vacuum and the residue was purified by flash column chromatography (silica gel; diethyl ether/pentane as the eluent) to afford (*S*)-2-bromo-*N*-(1-methoxy-3-phenylpropan-2-yl)aniline (1.36 g, 67% yield) as a colorless oil. ^{1}H NMR (400 MHz, $CDCl_3$): δ=3.02 (d, *J*=6.5 Hz, 1H), 3.40–3.50 (m, 3H), 3.81–3.87 (m, 1H), 4.67 (d, *J*=8.1 Hz, 1H), 6.62 (td, *J*=7.7, 1.4 Hz, 1H), 6.78 (dd, *J*=8.2, 1.1 Hz, 1H), 7.24 (ddd, *J*=8.4, 7.3, 1.4 Hz, 1H), 7.27–7.35 (m, 3H), 7.35–7.44 (m, 2H), 7.49 ppm (dd, *J*=7.9, 1.5 Hz, 1H); ^{13}C NMR (100 MHz, $CDCl_3$): δ=37.2, 54.0, 59.1, 72.5, 110.3, 111.7, 117.7, 126.5, 128.5, 129.5, 132.7, 138.1, 144.0 ppm; IR (neat): $\tilde{\nu}$=3402, 3026, 2923, 1739, 1593, 1505, 1454, 1431, 1366, 1319, 1231, 1202, 1119, 1069, 1016, 968, 738, 698, 638 cm^{-1}; HRMS (ESI): *m/z* calcd for $C_{16}H_{19}BrNO$ $[M+H]^+$: 320.0644; found: 320.0641.

(*S*)-2-Bromo-*N*-(1-methoxy-3-phenylpropan-2-yl)aniline (1.36 g, 4.25 mmol, 1 equiv) was dissolved in methyl chloroformate (3.5 mL, 45 mmol, 15 equiv). The reaction mixture was heated at reflux for 6 h before the reaction mixture was poured into ice/water and extracted with dichloromethane. The organic phase was dried over $MgSO_4$ and evaporated by means of a rotary evaporator after filtration. The crude product was purified by flash column chromatography (silica gel; ethyl acetate/pentane=1:30 as eluent) to afford (*S*)-**1x** as a colorless oil (1.54 g, 96%). $[\alpha]_D^{25}=-4.77$ (*c*=1.0 in CH_2Cl_2); ^{1}H NMR (400 MHz, $CDCl_3$): δ=2.62 (dd, *J*=13.3, 9.5 Hz, 1H), 3.19 (s, 1.8H), 3.25 (dd, *J*=13.2, 6.5 Hz, 1H), 3.37 (s, 4H), 3.45–3.68 (m, 1H), 3.65 (dd, *J*=10.0, 4.6 Hz, 1H), 3.71 (s, 1H), 3.72 (s, 3H), 3.77–3.94 (m, 1H), 4.22–4.29 (m, 0.5H), 4.45–4.52 (m, 1H), 6.97 (d, *J*=7.7 Hz, 1H), 7.13–7.43 (m, 11H), 7.64 (dd, *J*=8.0 Hz, 1H), 7.66 ppm (d, *J*=11.3, 0.5H); ^{13}C NMR (100 MHz, $CDCl_3$): δ=14.2, 21.1, 35.5, 37.3, 52.9, 53.0, 58.5, 58.6, 60.4, 61.4, 62.5, 70.6, 72.0, 124.8, 125.5, 126.4, 126.5, 128.0, 128.0, 128.5, 128.5, 128.6, 128.7, 129.2, 129.3, 130.9, 133.1, 138.7, 139.2, 155.1, 155.6 ppm; IR (neat): $\tilde{\nu}$=3027, 2950, 1706, 1584, 1474, 1440, 1297, 1190, 1116, 1067, 1028, 951, 761, 747, 700 cm^{-1}; HRMS (EI): *m/z* calcd for $C_{18}H_{20}BrNO_3$ $[M]^+$: 337.0621; found: 337.0615.

Catalytic asymmetric synthesis of (2*S*,3*R*)-2x

Carbamate (*S*)-**1x** (75.6 mg, 0.2 mmol), cesium carbonate (97.5 mg, 0.3 mmol), [{Pd(π-cinnamyl)Cl}$_2$] (2.6 mg, 0.005 mmol), cesium pivalate (46.8 mg, 0.2 mmol), and (*R*,*R*)-**5** (5.9 mg, 0.01 mmol) were placed in a Schlenk flask. After the flask was evacuated and backfilled with nitrogen, dry mesitylene (2 mL) was added under nitrogen. The resulting reaction mixture was stirred at 160 °C for 3 h. The reaction mixture was cooled to RT and diluted with dichloromethane (2 mL) followed by filtration through a pad of Celite. The filtrate was evaporated under high vacuum. The residue was purified by flash column chromatography (silica gel; ethyl acetate/pentane=1:30 as the eluent) to afford (2*S*,3*R*)-**2x** as a colorless oil (58.2 mg, 98%, >99% *ee*). $[\alpha]_D^{20}=-24.18$ (*c*=1.0 in CH_2Cl_2); ^{1}H NMR (400 MHz, $CDCl_3$): δ=2.47–2.58 (m, 1H), 3.08 (br s, 3H), 3.15–3.47 (m, 1H), 3.87 (br s, 3H), 4.43 (s, 1H), 4.50–4.61 (m, 1H), 7.12 (t, *J*=7.2 Hz, 1H), 7.20–7.51 (m, 2H), 7.51–8.14 ppm (m, 1H); ^{13}C NMR (100 MHz, $CDCl_3$): δ=38.0, 52.7, 55.2, 59.2, 66.2, 81.8, 115.9, 122.9, 126.6, 126.8, 127.4, 128.1, 128.6, 129.5, 130.5, 137.0 ppm; IR (neat): $\tilde{\nu}$=2952, 1704, 1603, 1481, 1440, 1389, 1346, 1316, 1272, 1190, 1136, 1087, 1055, 1034, 968, 755 cm^{-1}; HRMS (EI): *m/z* calcd for $C_{18}H_{19}NO_3$ $[M]^+$: 297.1360; found: 297.1359.

Catalytic asymmetric synthesis of (2*S*,3*S*)-3x

Carbamate (*S*)-**1x** (75.6 mg, 0.2 mmol), cesium carbonate (97.5 mg, 0.3 mmol), [{Pd(π-cinnamyl)Cl}$_2$] (2.6 mg, 0.005 mmol), cesium pivalate (46.8 mg, 0.2 mmol), and (*S*,*S*)-**5** (5.9 mg, 0.01 mmol) were placed in a Schlenk flask. After the flask was evacuated and backfilled with nitrogen, dry mesitylene (2 mL) was added under nitrogen. The resulting reaction mixture was stirred at 160 °C for 3 h. The reaction mixture was cooled to RT and diluted with dichloromethane (2 mL) followed by filtration through a pad of Celite. The filtrate was evaporated under high vacuum. The residue was purified by flash column chromatography (silica gel; ethyl acetate/pentane=1:30 as the eluent) to afford (2*S*,3*S*)-**3x** as a colorless solid (58.2 mg, 98%, >99% *ee*). M.p.=117–119 °C; $[\alpha]_D^{20}=+69.59$ (*c*=1.0 in CH_2Cl_2); ^{1}H NMR (400 MHz, $CDCl_3$): δ=3.46 (s, 3H), 3.53 (t, *J*=9.0 Hz, 1H), 3.76 (dd, *J*=9.4, 3.8 Hz, 1H), 3.89 (s, 3H), 4.49–4.52 (m, 2H), 7.01–7.18 (m, 4H), 7.24–7.34 (m, 4H), 7.46–8.13 ppm (br d, 1H); ^{13}C NMR (100 MHz, $CDCl_3$): δ=49.3, 52.7, 59.2, 67.2, 72.7, 115.4, 123.4, 126.0, 126.8, 127.4, 128.1, 128.7, 144.1 ppm; IR (neat): $\tilde{\nu}$=2929, 2818, 1703, 1599, 1481, 1440, 1377, 1302, 1261, 1189, 1136, 1122, 1047, 964, 760 cm^{-1}; HRMS (ESI): *m/z* calcd for $C_{18}H_{20}NO_3$ $[M+H]^+$: 298.1437; found: 298.1438.

Computational methods

Density functional (M06-L/LANL2DZ,6-31G(d,p)) calculations were used to study the CMD step of the C(sp^3)–H arylation. Single-point PCM calculations in xylenes of all gas-phase optimized structures yielded the solvent-corrected energy, E_{solv}.[25] The united atom topological model with UAHF radii was used. For the PCM calculations, the same level of theory as that used in the gas-phase calculations was used. Gas-phase Gibbs free energy corrections, G_{corr} (P=1 atm, T=298 K), were considered for each species and the total Gibbs free energy, G, of each optimized structure was taken as $G=E_{solv}+G_{corr}$. The calculations were performed with the Gaussian 09 package.[19]

Acknowledgements

We thank the Swiss National Science Foundation and the University of Geneva for financial support. E.L. expresses his thanks to Prof. H. Zipse for providing access to the Linux cluster at the Faculty of Chemistry and Pharmacy of the LMU Munich.

Keywords: asymmetric catalysis · carbenes · C–H activation · chirality · density functional calculations

[1] For recent reviews on C–H insertion, see: a) M. P. Doyle, R. Duffy, M. Ratnikov, L. Zhou, *Chem. Rev.* **2010**, *110*, 704 – 724; b) H. M. L. Davies, A. R. Dick, *Top. Curr. Chem.* **2010**, *292*, 303 – 345.

[2] A. R. Dick, M. S. Sanford, *Tetrahedron* **2006**, *62*, 2439 – 2463.

[3] For reviews on C–H bond functionalization, see: a) L. Ackermann, *Acc. Chem. Res.* **2014**, *47*, 281 – 295; b) Q.-Z. Zheng, N. Jiao, *Tetrahedron Lett.* **2014**, *55*, 1121 – 1126; c) P. B. Arockiam, C. Bruneau, P. H. Dixneuf, *Chem. Rev.* **2012**, *112*, 5879 – 5918; d) B.-J. Li, Z.-J. Shi, *Chem. Soc. Rev.* **2012**, *41*, 5588 – 5598; e) S. R. Neufeldt, M. S. Sanford, *Acc. Chem. Res.* **2012**, *45*, 936 – 946; f) N. Kuhl, M. N. Hopkinson, J. Wencel-Delord, F. Glorius, *Angew. Chem.* **2012**, *124*, 10382 – 10401; *Angew. Chem. Int. Ed.* **2012**, *51*, 10236 – 10254; g) L. Ackermann, *Chem. Rev.* **2011**, *111*, 1315 – 1345; h) X. Chen, K. M. Engle, D.-H. Wang, J.-Q. Yu, *Angew. Chem.* **2009**, *121*, 5196 – 5217; *Angew. Chem. Int. Ed.* **2009**, *48*, 5094 – 5115.

[4] For selected references, see: a) B. Biswas, M. Sugimoto, S. Sakaki, *Organometallics* **2000**, *19*, 3895 – 3908; b) S. Pascual, P. de Mendoza, A. M. Echavarren, *Org. Biomol. Chem.* **2007**, *5*, 2727 – 2734; c) D. Balcells, E. Clot, O. Eisenstein, *Chem. Rev.* **2010**, *110*, 749 – 823; d) S. Rousseaux, S. I. Gorelsky, B. K. W. Chung, K. Fagnou, *J. Am. Chem. Soc.* **2010**, *132*, 10692 – 10705; e) R. Jazzar, J. Hitce, A. Renaudat, J. Sofack-Kreutzer, O. Baudoin, *Chem. Eur. J.* **2010**, *16*, 2654 – 2672.

[5] C. Zheng, S.-L. You, *RSC Adv.* **2014**, *4*, 6173 – 6214.

[6] N. Dastbaravardeh, M. Christakakou, M. Haider, M. Schnürch, *Synthesis* **2014**, 1421 – 1439.

[7] T. Watanabe, S. Oishi, N. Fujii, H. Ohno, *Org. Lett.* **2008**, *10*, 1759 – 1762.

[8] M. Nakanishi, D. Katayev, C. Besnard, E. P. Kündig, *Angew. Chem.* **2011**, *123*, 7576 – 7579; *Angew. Chem. Int. Ed.* **2011**, *50*, 7438 – 7441.

[9] S. Anas, A. Cordi, H. B. Kagan, *Chem. Commun.* **2011**, *47*, 11483.

[10] a) T. Saget, S. J. Lemouzy, N. Cramer, *Angew. Chem.* **2012**, *124*, 2281 – 2285; *Angew. Chem. Int. Ed.* **2012**, *51*, 2238 – 2242; b) T. Saget, N. Cramer, *Angew. Chem.* **2012**, *124*, 13014 – 13017; *Angew. Chem. Int. Ed.* **2012**, *51*, 12842 – 12845; c) T. Saget, D. Perez, N. Cramer, *Org. Lett.* **2013**, *15*, 1354 – 1357.

[11] N. Martin, C. Pierre, M. Davi, R. Jazzar, O. Baudoin, *Chem. Eur. J.* **2012**, *18*, 4480 – 4484.

[12] E. Larionov, M. Nakanishi, D. Katayev, C. Besnard, E. P. Kündig, *Chem. Sci.* **2013**, *4*, 1995 – 2005.

[13] D. Katayev, M. Nakanishi. T. Bürgi, E. P. Kündig, *Chem. Sci.* **2012**, *3*, 1422 – 1425.

[14] For a review on divergent reactions on racemic mixtures, see: L. C. Miller, R. Sarpong, *Chem. Soc. Rev.* **2011**, *40*, 4550 – 4562.

[15] a) J. F. Hartwig, *Acc. Chem. Res.* **2008**, *41*, 1534 – 1544; b) D. S. Surry, S. L. Buchwald, *Chem. Sci.* **2011**, *2*, 27 – 50.

[16] a) S. Rousseaux, B. Liegault, K. Fagnou, *Chem. Sci.* **2012**, *3*, 244 – 248; b) C. Tsukano, M. Okuno, Y. Takemoto, *Angew. Chem.* **2012**, *124*, 2817 – 2820; *Angew. Chem. Int. Ed.* **2012**, *51*, 2763 – 2766; c) C. Tsukano, M. Okuno, Y. Takemoto, *Chem. Lett.* **2013**, *42*, 753 – 755; d) Q. Zhang, H.-Z. Yu, Y. Fu, *Organometallics* **2013**, *32*, 4165 – 4173.

[17] CCDC-1008423 ((2*S*,3*S*)-**3x**) contains the supplementary crystallographic data for this paper. These data can be obtained free of charge from The Cambridge Crystallographic Data Centre via www.ccdc.cam.ac.uk/data_request/cif.

[18] a) M. Lafrance, K. Fagnou, *J. Am. Chem. Soc.* **2006**, *128*, 16496 – 16497; b) M. Lafrance, S. I. Gorelsky, K. Fagnou, *J. Am. Chem. Soc.* **2007**, *129*, 14570 – 14571.

[19] Gaussian 09, Revision A.02, M. J. Frisch, G. W. Trucks, H. B. Schlegel, G. E. Scuseria, M. A. Robb, J. R. Cheeseman, G. Scalmani, V. Barone, B. Mennucci, G. A. Petersson, H. Nakatsuji, M. Caricato, X. Li, H. P. Hratchian, A. F. Izmaylov, J. Bloino, G. Zheng, J. L. Sonnenberg, M. Hada, M. Ehara, K. Toyota, R. Fukuda, J. Hasegawa, M. Ishida, T. Nakajima, Y. Honda, O. Kitao, H. Nakai, T. Vreven, J. A. Montgomery, Jr., J. E. Peralta, F. Ogliaro, M. Bearpark, J. J. Heyd, E. Brothers, K. N. Kudin, V. N. Staroverov, R. Kobayashi, J. Normand, K. Raghavachari, A. Rendell, J. C. Burant, S. S. Iyengar, J. Tomasi, M. Cossi, N. Rega, J. M. Millam, M. Klene, J. E. Knox, J. B. Cross, V. Bakken, C. Adamo, J. Jaramillo, R. Gomperts, R. E. Stratmann, O. Yazyev, A. J. Austin, R. Cammi, C. Pomelli, J. W. Ochterski, R. L. Martin, K. Morokuma, V. G. Zakrzewski, G. A. Voth, P. Salvador, J. J. Dannenberg, S. Dapprich, A. D. Daniels, Ö. Farkas, J. B. Foresman, J. V. Ortiz, J. Cioslowski, D. J. Fox, Gaussian, Inc. Wallingford CT, **2009**.

[20] a) S. Grimme, *J. Comput. Chem.* **2004**, *25*, 1463 – 1473; b) S. Grimme, *J. Comput. Chem.* **2006**, *27*, 1787 – 1799.

[21] a) A. F. Abdel-Magid, K. G. Carson, B. D. Harris, C. A. Maryanoff, R. D. Sarah, *J. Org. Chem.* **1996**, *61*, 3849 – 3862; b) D. J. Cho, C. J. Wu, S. S, W.-S. Han, S. O. Kang, B. Y. Lee, *Organometallics* **2006**, *25*, 2133 – 2134.

[22] N. Marion, O. Navarrro, J. Mei, E. D. Steven, N. M. Scott, S. P. Nolan, *J. Am. Chem. Soc.* **2006**, *128*, 4101 – 4111.

[23] For the synthesis of (*S*,*S*)- and (*R*,*R*)-**4**, see: E. P. Kündig, T. M. Seidel, Y. X. Jia, G. Bernardinelli, *Angew. Chem.* **2007**, *119*, 8636 – 8639; *Angew. Chem. Int. Ed.* **2007**, *46*, 8484 – 8487; (*S*,*S*)- and (*R*,*R*)-**5**: D. Katayev, Y.-X. Jia, A. K. Sharma, D. Banerjee, C. Besnard, R. B. Sunoj, E. P. Kündig, *Chem. Eur. J.* **2013**, *19*, 11916 – 11927; (*S*,*S*)-**4** and (*S*,*S*)-**5** are available from Sigma-Aldrich Corporation.

[24] (*S*)-1-Methoxy-3-phenylpropan-2-amine was synthesized according to a procedure reported in the literature, see: B. Deng, Q. Wu, Y. Pan, B. Hu, L. Zhang, Patent CN 102060732 (A), **2011**.

[25] J. Tomasi, B. Mennucci, R. Cammi, *Chem. Rev.* **2005**, *105*, 2999 – 3094.

Received: June 16, 2014
Published online on September 26, 2014